

# PETROPHYSICAL EVALUATION OF ARKOSES RESERVOIRS BASED ON WELL LOGS AND PLUG SAMPLES: A CASE STUDY FROM ALAGAMAR FORMATION, SOUTHEASTERN PORTION OF ONSHORE POTIGUAR BASIN, BRAZIL

Victor Ferreira<sup>1</sup>, Antonio Fernando Menezes Freire<sup>2</sup> and Wagner Moreira Lupinacci<sup>2</sup>

<sup>1</sup>3R Petroleum, Reservoir Department, Praia de Botafogo, 186 - Botafogo, Rio de Janeiro - RJ, Brazil

<sup>2</sup>Universidade Federal Fluminense - UFF, Campus da Praia Vermelha, Niterói, RJ, Brazil

\*Corresponding author email: [victorhlimaf@gmail.com](mailto:victorhlimaf@gmail.com)

**ABSTRACT.** The Potiguar Basin is a sedimentary basin located in northeastern Brazil. It covers about 48,000 km<sup>2</sup> and extends from onshore to offshore. The onshore basin is thought to have formed during the Late Cretaceous, as a result of the opening of the Equatorial South Atlantic Ocean, filled with a thick sequence of sedimentary rocks, including sandstones, shales, and limestones, which were deposited in a variety of processes, including marine, deltaic, and fluvial. The study area is in the southern portion of the basin and the reservoir is composed of arkose sandstones deposited by alluvial fan and fluvial systems of the Upanema Member of the Alagamar Formation, which belongs to the post-rift phase of the Potiguar Basin. Recently, new drilling campaigns revealed a reservoir heterogeneity in these deposits, which requested a new petrophysical approach. Using conventional well logs and petrophysical laboratory analysis of plug samples, this study evaluated the best way to calculate the effective porosity, and shale volume and to understand the stratigraphic controls in the distribution of these properties. Three reservoir zones were mapped: the basal one, Zone 3, has disconnected sand bodies, low porosity, and high shale content; Zone 2 has better petrophysical properties, lateral distribution, and connectivity between the fans and Zone 1 is the better reservoir zone with larger sand bodies, higher porosity values, and well-connected fans.

**Keywords:** Formation evaluation, Shale volume, Net Sand, Spectral Gamma ray.

## INTRODUCTION

The onshore Potiguar Basin has been explored for oil and gas since the 1970s and several large fields have been discovered and developed. Recently, several authors have been studying and reanalyzing the basin's stratigraphy in the seismic and reservoir scale (Anjos et al., 2000; Monteiro, 2012; Melo et al., 2019; Melo et al., 2021), mainly the Pendência and Açú formations,

and its tectonic events (Bertani et al., 1990; Matos, 1992; Bezerra & Vita-Finzi, 2000; Nogueira et al., 2010; De Castro et al., 2012; De Castro & Bezerra, 2015; Bezerra et al., 2019).

However, in the study area, the main producer is in the Alagamar Formation, specifically in the Upanema Member sandstones deposited in alluvial-fluvial environmental conditions (Araripe and Feijó, 1994; Pessoa Neto et al., 2007), and little has been published about this sedimentary section using well logs.

The characterization of heterogeneities and the understanding of their distribution play an important role when planning the development of an oil and gas field. In alluvial fans and fluvial depositional systems, these heterogeneities could manifest in the form of discontinuous sand bodies with high variations in reservoir qualities (porosity and permeability, mainly), making reservoir zonation a challenging task for reservoir geologists. Therefore, to better understand the petrophysical properties distribution and their link with the depositional environment, it is important to integrate rock sample data with the well log analysis.

The sandstones of the Upanema Member, in the study area, have a significant feldspar content, and, consequently, gamma ray (GR) logs show higher values in arkoses than other reservoirs with high quartz content. This factor makes it difficult to identify the difference between clean sandstones and shaly intervals in GR. For this reason, the shale volume ( $V_{shale}$ ) was calculated using several methods such as Larionov Old Rocks and Paleogene Rocks (Larionov, 1969), Clavier *et al.* (1984), and Stieber (1970).

Considering these calculations, we use each  $V_{shale}$  ( $V_{sh}$ ) method to calculate the effective porosity and then correlate it with the one measured in plug samples. By doing so, identifying the best way to estimate clay volume and using this method in each zone for all 74 wells, and, finally, using kriging to distribute it in the study area. We propose Net Sand maps to identify the petrophysical properties distribution, associated with the alluvial fan's distribution, and use it to identify possible stratigraphic limits due to its lateral continuity for each reservoir zone in the study area.

In addition to the conventional logs, this work also proposes the use of spectral gamma ray logs with Th/K, Th/U, and K/U ratios to characterize clay minerals present in the reservoir zones.

### **Geological Setting**

The study area is located in the southeastern portion of the Potiguar Basin, Brazil (see Fig. 1). The wells correlation and studied interval are limited on the base of the Lower Alagoas Unconformity (LCU), which represents the erosion of the upper portion of the Pendência Formation in the Potiguar Basin, and on the base by the Lower Aptian Unconformity (LCA), that

represents the top of Alagamar Formation (Fig. 2).

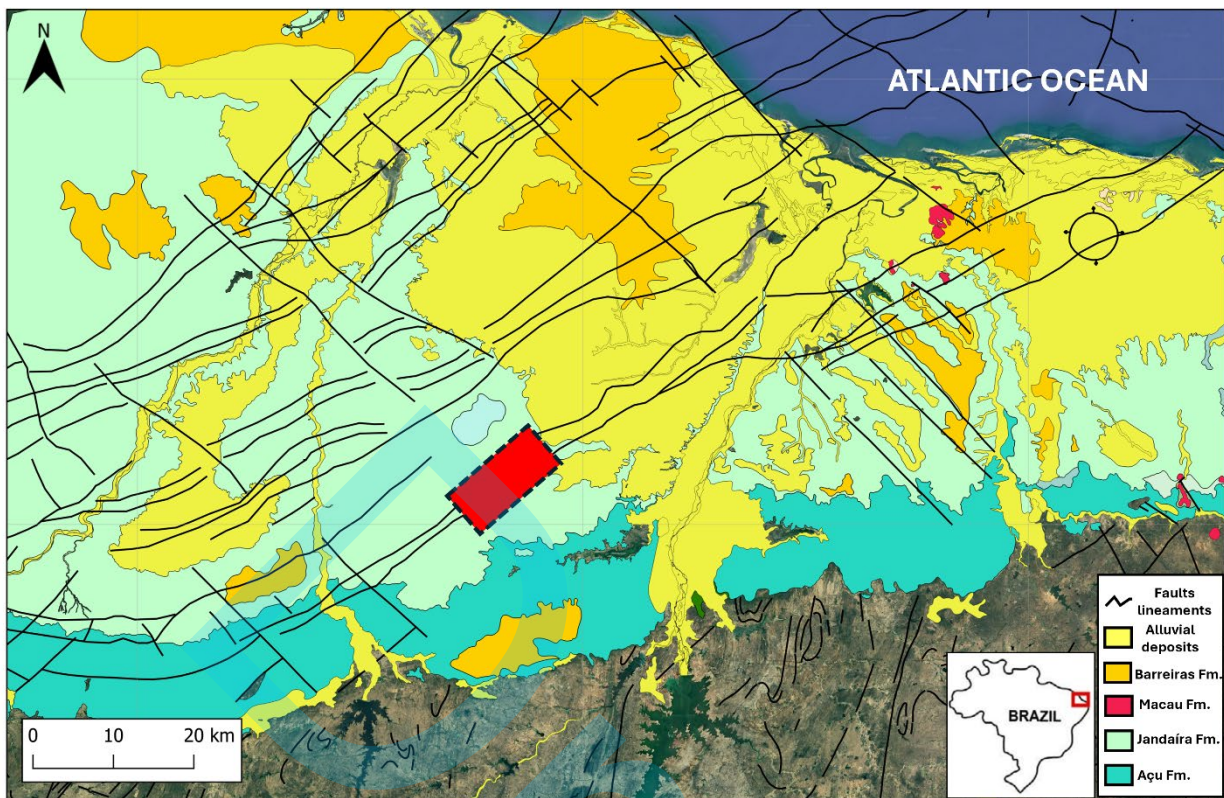


**Figure 1** – Regional Potiguar showing the studied area (red rectangle) and the regional fault lineaments (in black). The Neogene rocks and deposits, Açu and Jandaíra formations crop out in the onshore section of the basin. Modified from Bertani et al. (1990), Angelim et al. (2006), and De Castro & Bezerra (2015).

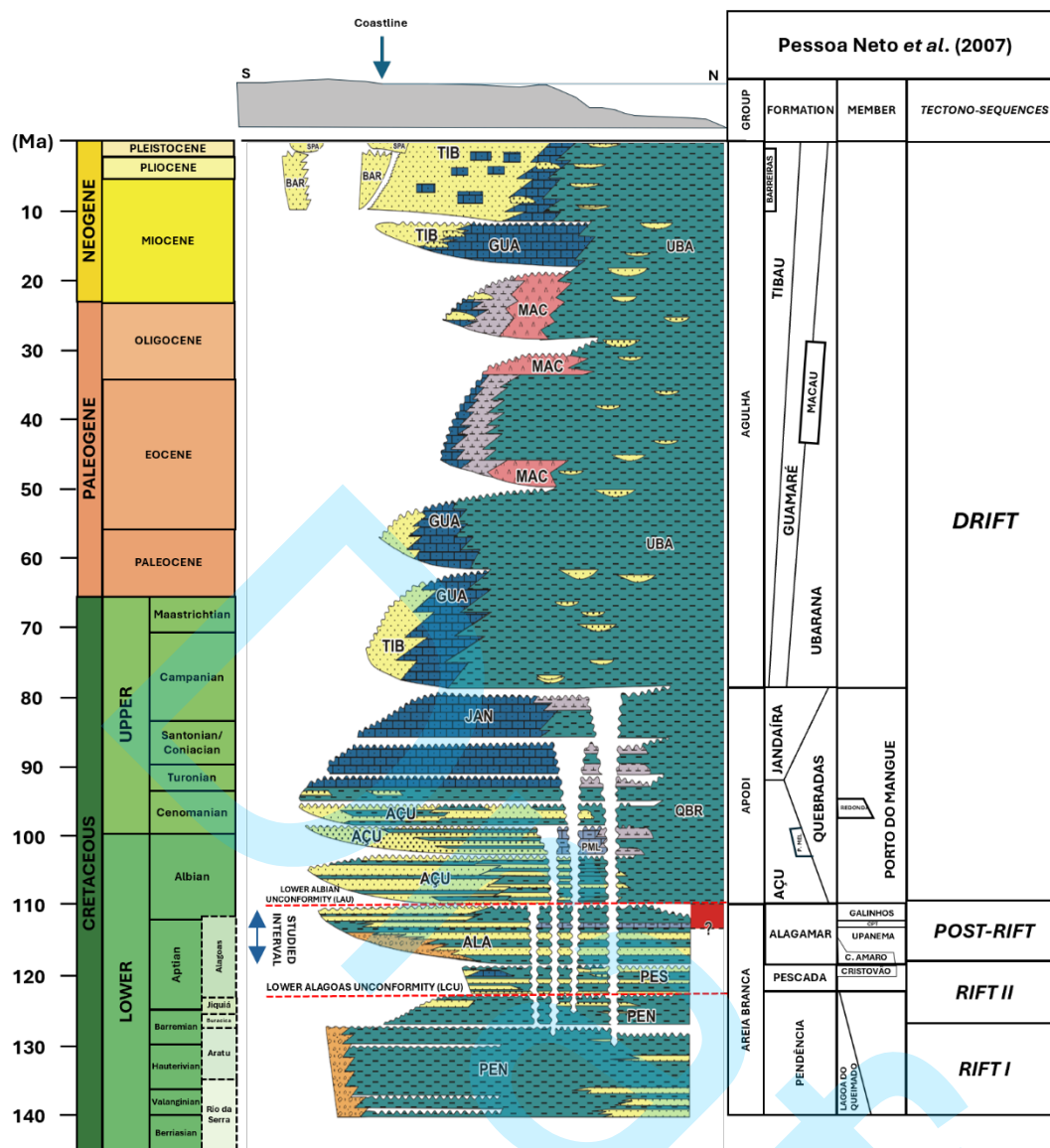


**Figure 2** – Potiguar Basin stratigraphic chart illustrating the different evolutionary stages. The Alagamar Formation is located between two unconformities: Lower Alagoas Unconformity (LCU) and Lower Aptian Unconformity (LAU) (red lines in the chart). The Potiguar Basin is subdivided into 4 tectono-sequences, and the studied interval (blue arrow) comprises all the sedimentary records of the post-rift stage. Modified from Pessoa Neto et al. (2007).

The Alagamar Formation is composed of sediments deposited between the Late Aptian and Early Albian, and it marks the change from continental depositional systems to marine between rift and drift tectono-sequences (Araripe & Feijó, 1994). The dominant tectonic regime, known as the post-rift phase or transitional, had thermic subsidence as the main space generator mechanism.

This geological formation is subdivided into, from base to top, alluvial-deltaic systems (Canto do Amaro Member), alluvial-fluvial-deltaic systems (Upanema Member), and transitional shaly sandstones and shales (Galinhos Member). The maximum transgression composed of black

shales and marls, distributed in almost all the emerged portion of the basin, are known as Camadas Ponta Tubarão (CPT) marking the first marine incursions in the onshore portion of the basin (Araripe & Feijó, 1994, and Pessoa Neto *et al.*, 2007), and working as the seal beds of the studied reservoirs.

As the study area is located next to the Carnaubais' Fault System, as shown in Figure 2, the reservoirs are mainly proximal alluvial fans and fluvial sandstones close to the basement of the basin that worked as a sediment source for those deposits. These sandstones are from Upanema Member and are described as arkoses and lithic arkoses, poorly sorted and compositional deposits (Pessoa Neto *et al.*, 2007) (Fig. 3).

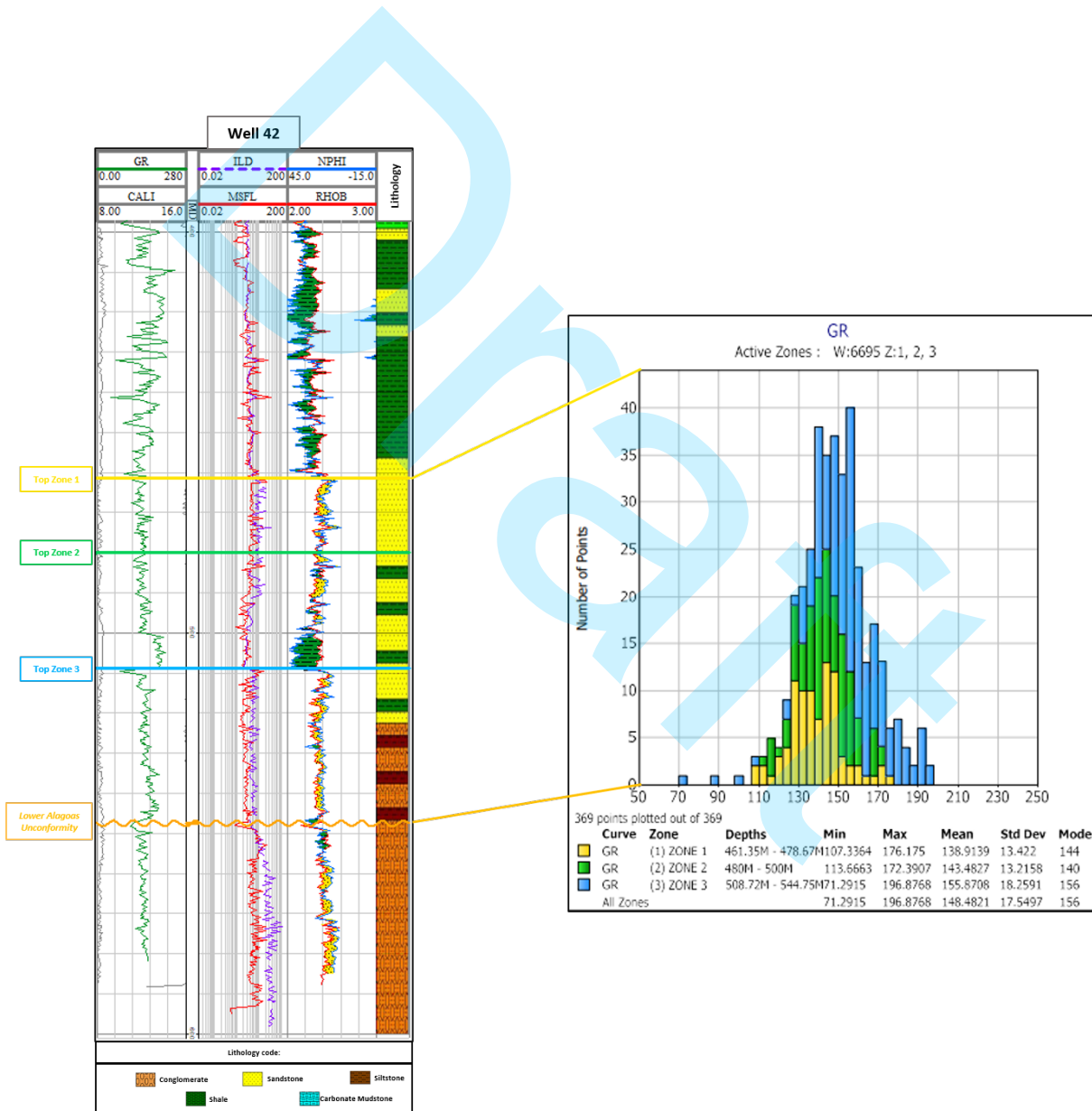


**Figure 3** –Well 42 with GR/CALI in track 1, ILD/MSFL in track 2, NPHI/RHOB in track 3, and mud logging in track 4. On the right, there is the histogram of GR values colored by the respective zone color (Zone 3 in blue, Zone 2 in green, and Zone 1 in yellow).

## DATASET AND METHODOLOGY

### Dataset

The study is based on a dataset derived from 74 wells drilled in one field located in the Southeastern portion of the Potiguar Basin (Fig. 4). We used the basic suite well logs gamma ray (GR), resistivity induction logs (ILD for deep resistivity and ILM for medium), density (RHOB), neutron (NPHI), sonic (DT), micro-resistivity (MSFL), photo-electric (PE), and spectral gamma ray logs (SGR – composed by K (%), U (ppm), Th (ppm) concentration logs – present in 13 wells). Available mud logging data was also used. All the calculations and log plotting were done in Python, S&P Kingdom®, and Techlog®.

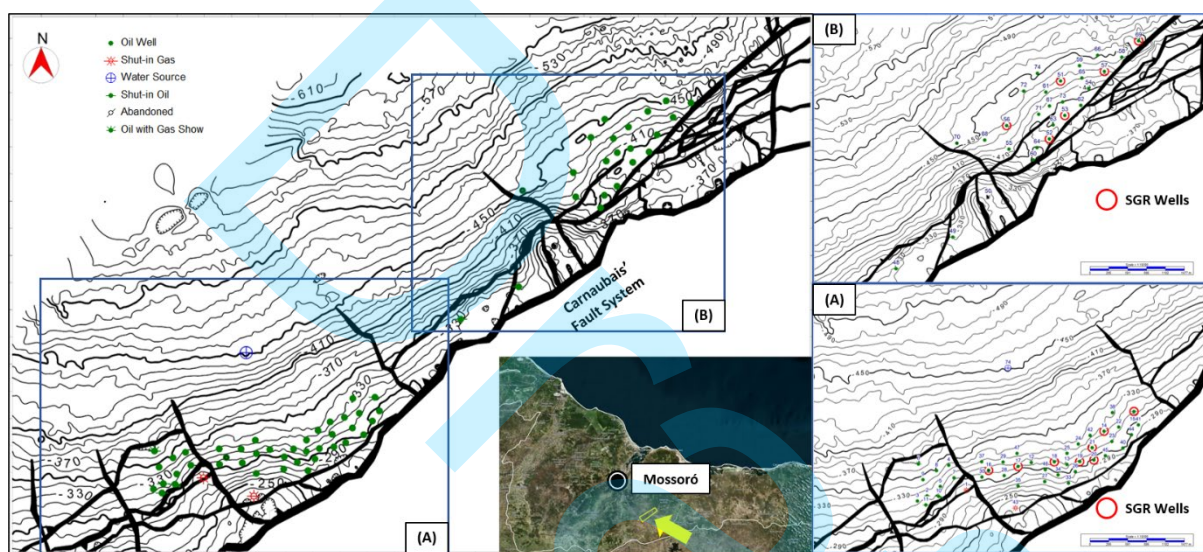


**Figure 4** – Location map of the study area in the southeastern portion of Potiguar Basin. Wells with spectral gamma ray logs are highlighted in red. A) Group of wells in the southwestern area. B) Group of wells in the northeastern portion of the study area.

From this dataset, four wells were cored, and from these cores, 94 plug samples were made and sent to petrophysical laboratory analysis with only five X-ray diffraction (XRD) analysis data available (Table 1). Unfortunately, the wells that have XRD data were not logged with spectral gamma rays.

**Table 1** – X-ray diffraction analysis from Wells 52 and 73 in five different plug samples and their respective mineral concentrations and depth. The presence of kaolinites, illites, and mixed illites/smectites was identified as the main clay minerals with concentrations up to 25% of the total rock mineral composition. It is important to note that Well 52 has a considerably higher concentration of mixed-layer clay (illite/smectite) than Well 73. Both have similar values of carbonates, quartz, k-feldspars, and plagioclase.

Well	Plug Sample	Depth (m)	Clay Minerals				Carbonates		Other minerals				TOTAL		
			Chlorite	Kaolinite	Illite/Mica	Mixed Illite/Smectite	Calcite	Siderite	Quartz	K-Feldspars	Plagioclase	Pyrite	Clays	Carbonates	Others
52	1	511.9	Tr	Tr	1	24	2	0	32	31	9	1	25	2	73
	2	544.3	Tr	Tr	1	15	3	0	40	34	7	Tr	16	3	81
	3	568.7	Tr	2	1	7	6	0	36	34	14	Tr	10	6	84
73	4	555.5	0	1	7	2	1	1	44	22	19	0	10	2	90
	5	557.9	0	2	7	0	0	0	33	26	29	1	8	0	92
<b>AVERAGE</b>			0	2	3	10	2	0	37	29	16	1	14	3	84

\*Tr = trace mineral concentration below 1% and not considered for the average calculation.

## Theoretical Foundation

The first workflow is the initial quality control for the log curves, followed by the reservoir zonation and well correlation separating the sandstone intervals from the shales using the conventional well logs. After the zonation, the first step is to establish the best clay volume equation to use before calculating the effective porosity. To do so, the Gamma Ray Index (IGR or APIGR) is calculated by Eq. (1) (Schlumberger, 1974):

$$IGR = \frac{GR - GR_{min}}{GR_{max} - GR_{min}} \quad (1)$$

, where:

- IGR is the volume of shale,
- $GR$  is the gamma ray reading of the formation,
- $GR_{min}$  is the minimum gamma ray reading in the formation (usually found in the cleanest sandstone or limestone layers),
- $GR_{max}$  is the maximum gamma ray reading in the formation (usually found in the purest shale layers).

This equation assumes that the gamma-ray log response of the cleanest sandstone or limestone layer represents the minimum, while maximum gamma-ray values represent shaly intervals, respectively, for a given formation. The equation calculates the shale volume by comparing the gamma-ray response of the formation to these reference values. This equation is widely used and has been developed and refined over time by petrophysicists and geoscientists through the analysis of numerous well logs and field data.

After calculating the IGR,  $V_{sh}$  was calculated using several methods like Larionov Old Rocks & Larionov Paleogene Rocks (Larionov, 1969), Clavier et al. (1984), and Stieber (1970) represented by Eq. (2), (3), (4) and (5):

$$Vsh_{LarionovOldRocks} = 0.33 \times (2^{2 \times IGR} - 1) \quad (2)$$

$$Vsh_{LarionovPaleogeneRocks} = 0.083 \times (2^{3.7 \times IGR} - 1) \quad (3)$$

$$Vsh_{Clavier} = 1.7 - (3.38 - (IGR + 0.7))^{\frac{1}{2}} \quad (4)$$

$$Vsh_{Stieber} = \frac{IGR}{3 - 2 \times IGR} \quad (5)$$

An additional significant technique for the estimation of Vsh involves the utilization of the neutron-density model as introduced by Bhuyan and Passey (1994). Nevertheless, this approach was not applied within the context of the present study, attributable to the elevated levels of gas saturation found within the zones of the examined reservoir. This divergence arises from the pronounced sensitivity of the neutron log to the heightened hydrogen content within the clay constituents, in contrast to the density log (Paiva et al., 2019).

After calculating the shale volume using these different methods, the next step was to estimate the total porosity ( $\phi$ ) and effective porosity ( $\phi_{Effective}$ ). Porosity could be calculated through the density (RHOB) and/or neutron (NPHI) log. To convert bulk density to total porosity, there is a widespread industry formula (eq. 6):

$$\phi_{RHOB} = \frac{RHOMA - RHOB}{RHOMA - RHOF} \quad (6)$$

where:

- $\phi_{RHOB}$  = porosity from density log,
- $RHOMA$  = matrix density,
- $RHOB$  = formation bulk density (log value),
- $RHOF$  = density of the fluid saturating the rock immediately surrounding the borehole – usually mud filtrate (1.11 for saltwater mud in this study).

Neutron energy loss can be related to porosity because, in porous formations, hydrogen is concentrated in the fluid filling the pores. Reservoirs whose pores are gas-filled may have a lower porosity than the same pores filled with oil or water because gas has a lower concentration of hydrogen atoms than either oil or water. So, the neutron log values are used as total porosity ( $\phi_{NPHI}$ ).



Once the density porosity is calculated, it is corrected by the shale content according to the following expression (Schlumberger, 1974) (eq. 7):

$$\Phi_{D_{corrected}} = \Phi_D - \left[ \left( \frac{\Phi_{D_{sh}}}{0.45} \right) \times 0.13 \times V_{sh} \right]$$

Next, the corrected density-derived porosity  $\Phi_{D_c}$  is combined with the corrected neutron porosity  $\Phi_{N_c}$  to estimate the neutron density porosity  $\Phi_{ND}$  (Schlumberger, 1974) (eq. 8):

$$\Phi_{N_{corrected}} = \Phi_N - \left[ \left( \frac{\Phi_{N_{sh}}}{0.45} \right) \times 0.03 \times V_{sh} \right]$$

$$\Phi_{ND} = \sqrt{\frac{\Phi_{N_c}^2 + \Phi_{D_c}^2}{2}}$$

Where  $\Phi_N$  is the neutron derived porosity (neutron log reading in decimal units) and  $\Phi_{N_{sh}}$  is the neutron porosity at a nearby shale.

$$\phi_{Total} = \left( \frac{(\phi_{NPHI}^2 + \phi_{RHOB}^2)}{2} \right)^{\frac{1}{2}} \quad (7)$$

There are various definitions of 'effective' porosity e.g. Juhasz (1986), Hill-Shirley-Klein (1979), and Clavier, et al. (1984). However, the most common definition is from Schlumberger (1987), (equation 11):

$$\phi_{Effective} = \phi_{Total} \times (1 - V_{shale})$$

The effective porosity is the porosity that excludes isolated pores and the volume occupied by water adsorbed on clay minerals (clay-bound water) and is the porosity used to calculate the water saturation in this evaluation.

This equation was used to calculate  $\phi_{Effective}$  for each one of the  $V_{shale}$  methods and then correlated with the  $\phi$  measured in the plug samples. After calculating the  $\phi_{Effective}$  for each well, the following cut-offs were defined to estimate the Net Sand intervals to generate maps and understand the distribution of the reservoir quality heterogeneities:

- $\phi_{Effective} > 10\%$
- $V_{shale} < 50\%$

The  $\phi_{Effective}$  cut-off was determined using the core analysis data, where the samples with less than 10% of  $\phi$  has very low permeability (close to 1mD) when compared to the other ones (see Fig. 5).

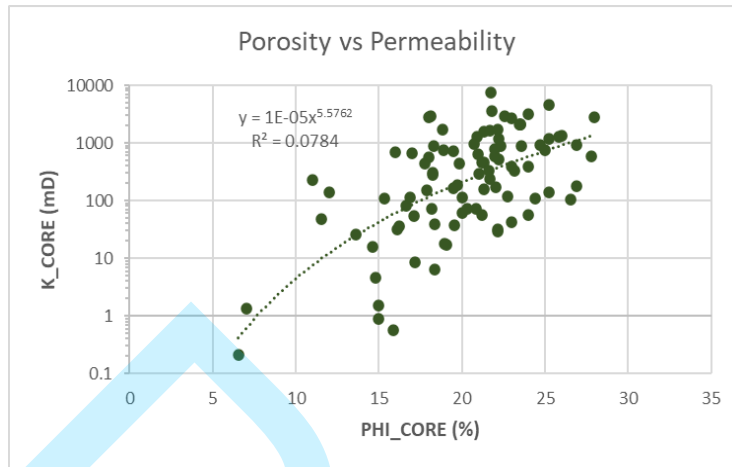


**Figure 5** – Correlation between the petrophysical laboratory measurement of effective porosity in 94 plug samples in four wells (PHI\_CORE) and the permeability (K\_CORE) also measured in these samples.

After understanding the thickness and distribution of the sandy bodies, another important step of the petrophysical evaluation is trying to identify and characterize the shaly intervals that work, or not, as fluid-flow barriers inside and between the mapped reservoir zones. In this workflow (Fig. 6), spectral gamma-ray logs play an important role when working with arkoses, which naturally have higher radioactivity than the siliceous ones, because of the presence of a  $^{40}K$  isotope.

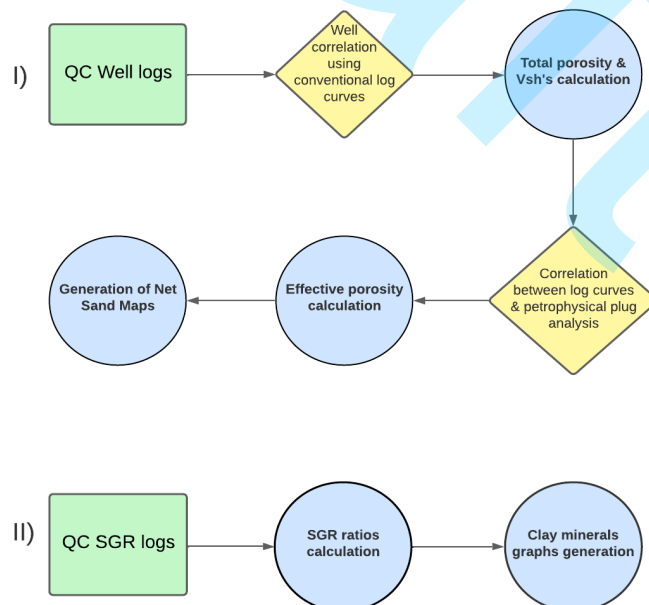


**Figure 6** – I) Workflow for the petrophysical evaluation and stratigraphic correlation between the reservoir zones; II) Workflow for the SGR logs evaluation aiming a better clay minerals characterization.

The natural gamma-ray spectrometry tools detect naturally occurring gamma rays of various energies emitted from a geological formation. Amounts and types of elements present are determined by how the formation was deposited and what has happened to it since deposition. These elemental concentrations thus calculated showed a correlation to depositional environment, geomorphic and diagenetic processes, clay type, and clay volume (Serra et al., 1980).

Radioactive isotopes initially contained mainly in acidic igneous rocks are transported due to geological processes to the sediments where they usually accumulate in a clayey substance. Typically, the high gamma ray response indicates the presence of fine-grained deposits or clay-rich formations, such as shale, claystone, and mudstone, while the relatively low gamma radiation indicates the presence of coarse-grained clean sandstones and carbonate rocks. However, the main feature of SGR is the ability to distinguish gamma emissions from  $^{40}\text{K}$ ,  $^{238}\text{U}$ , and  $^{232}\text{Th}$  (Klaja & Dudek, 2016).

The recognition of radioactive minerals, especially clay minerals present in the rocks, and the understanding of the oxidizing and reducing conditions of the depositional environment through the measurement of uranium (oxidizing environments are free of uranium while reducing environments are rich) allow a better determination of the mineralogical aspects. When combined with the vertical distribution of lithologies and grain sizes, it helps to reconstruct the depositional environment more accurately (Hassan et al., 1976).

Besides identifying those barriers through SGR logs, characterizing what type of clay minerals are present in the reservoir intervals is also important (in order to avoid expansive clays, e.g.). To do so, Schlumberger (1976 & 2009) and Doveton (1994 apud Bhattacharya & Carr, 2016) established, through empirical experiments, some graphics relating different types of clay minerals using PE, K (%), U (ppm), Th (ppm), and the ratios Th/K, and Th/U.

## RESULTS AND DISCUSSION

### Reservoir's $V_{sh}$ and Porosity evaluation

After calculating the effective porosity using all four  $V_{sh}$  methods for the four wells that were cored and plugged, the correlation between them was analyzed in Figure 7. The method that best fit for this dataset was  $V_{shale}$  calculation through Larionov Paleogene Rocks (Larionov, 1969), with an  $R^2$  of almost 0.97. After choosing Larionov Paleogene Rocks as the best way to estimate  $\phi_{Effective}$ , this petrophysical parameter was calculated for the 69 remaining wells. The distribution of this property could be analyzed in the histograms generated for all 3 zones in the 74 wells (see Fig. 8).

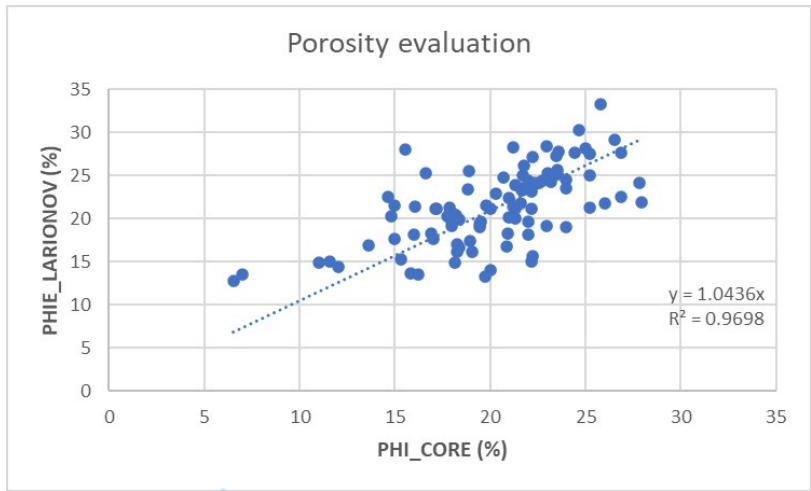


**Figure 7** – Correlation between the petrophysical laboratory measurement of effective porosity in 94 plug samples in four wells (PHI\_CORE) and the effective porosity calculated using the Larionov Paleogene Rock method (PHIE\_LARIONOV).

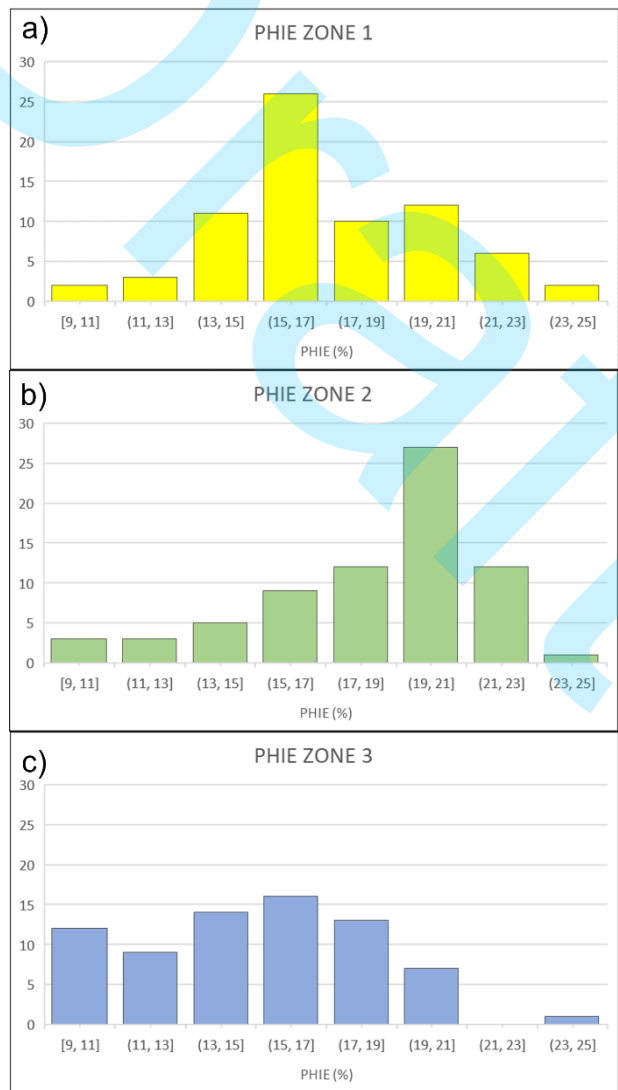


**Figure 8** – Histograms of effective porosity calculated for all the wells in the study area: (a) PHIE ZONE

1 - histogram for the top reservoir zone; (b) PHIE ZONE 2 - histogram for the intermediary zone, and; (c) PHIE ZONE 3 - histogram for the basal zone.

In Zone 3, the basal one, it's notable that most of the  $\phi$  *Effective* calculated were lower than the other two zones, which can result in worst productions from this zone. The other two zones have better  $\phi$  *Effective* values, and Zone 2 has the highest ones.

To understand the distribution of sand bodies with the best reservoir properties in the study area, Net Sand maps were generated (Figs. 9, 10, and 11) together with contour and structural maps of each reservoir. The basal map, from Zone 3, has better reservoir properties to the basinward, in the northwestern direction. In the Zone 2 map, the good reservoir properties are thicker and concentrated close to the Carnaubais' Fault System (CFS). The Zone 1 map shows not only that the sand bodies are also thicker and concentrated next to the CFS, but also more continuous laterally.

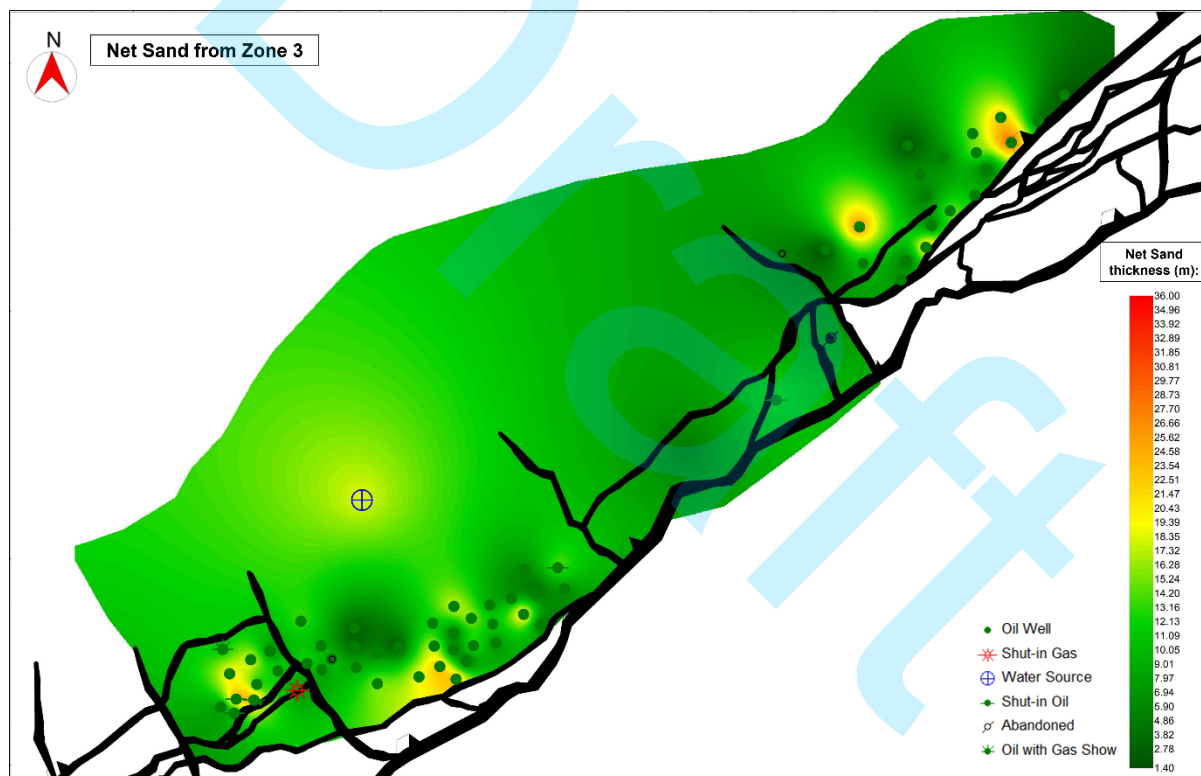


**Figure 9** – Isopach Net Sand Map colored below the faults for the basal reservoir (Zone 3) generated using the cut-off of 10% for PHIE values and <50% for  $V_{sh}$ . The well data was interpolated using kriging geostatistical method. The thicker net sand values seem to go basinward, in the northwestern direction. This figure made in S&P Kingdom software.

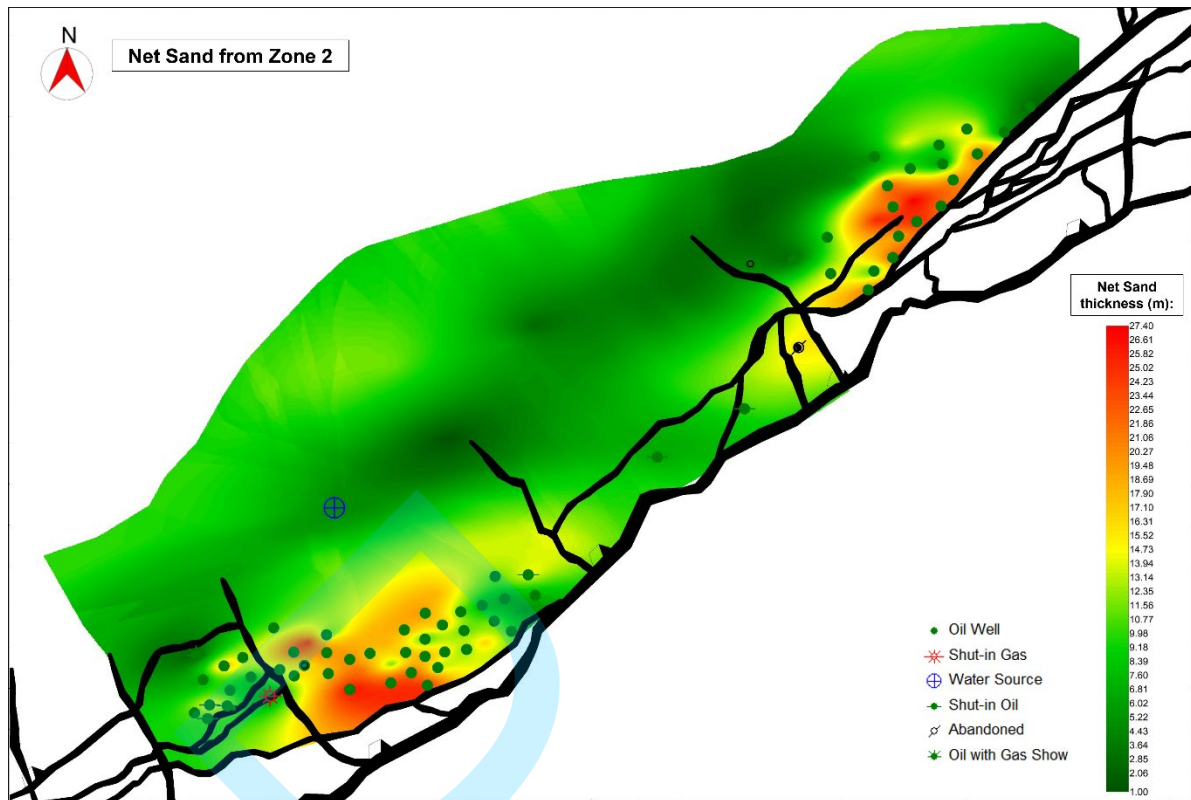


**Figure 10** – Isopach Net Sand Map coloured below the faults for the intermediary reservoir (Zone 2) generated using the cut-off of 10% for PHIE values and <50% for  $V_{sh}$ . The well data was interpolated using kriging geostatistical method. The portions with thicker net sand values are concentrated near the Carnaubais Fault System showing an geometry very similar to alluvial fans. This figure made in S&P Kingdom software.

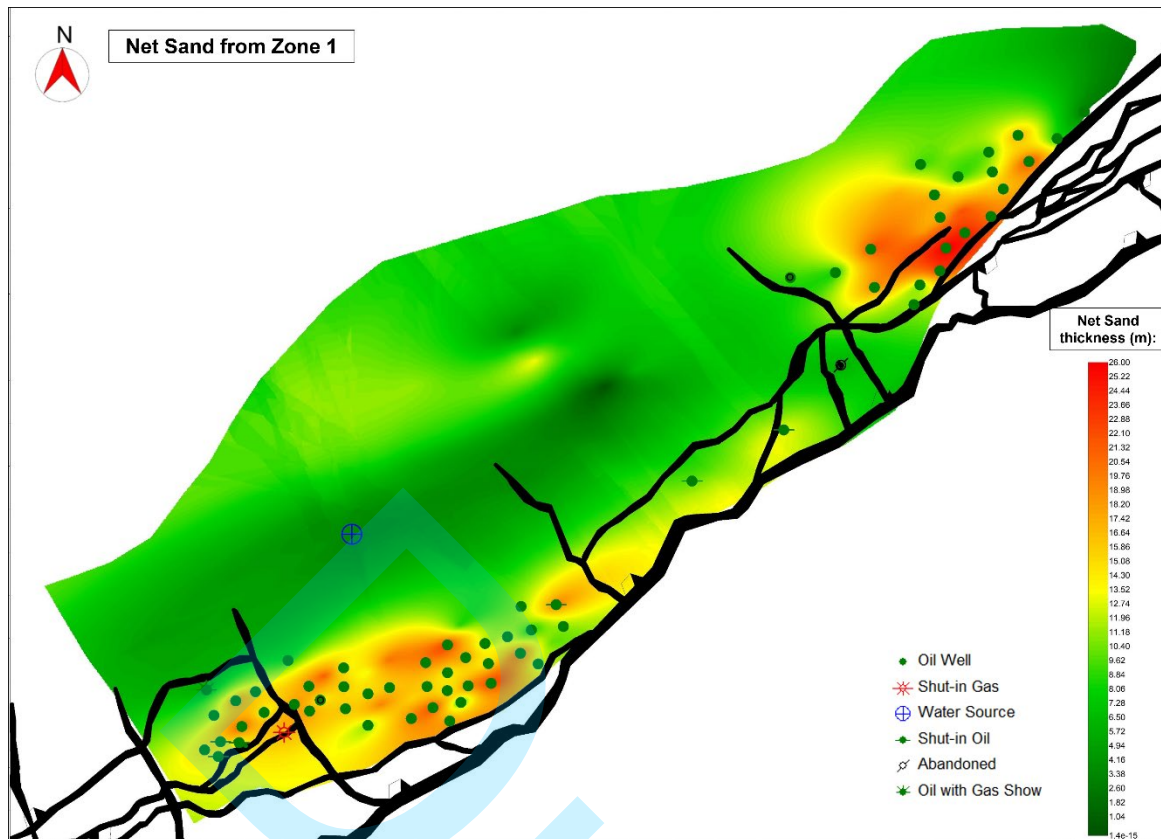


**Figure 11** – Isopach Net Sand Map coloured below the faults for the top reservoir (Zone 1) generated using the cut-off of 10% for PHIE values and <50% for  $V_{sh}$ . The well data was interpolated using kriging geostatistical method. The portions with thicker net sand values are concentrated near the Carnaubais Fault System, like the intermediary zone map, but with a better lateral continuity parallel to this fault system. This figure made in S&P Kingdom software.

As the Upanema Member, in the Alagamar Formation, is classified as a succession of flooding events in the post-rift phase of Potiguar Basin, the higher concentration of the sand bodies next to CFS in zones 2 and 3 could be linked to these flooding events. To understand these events, the Th (ppm) log was used to identify parasequences and sequence boundaries (Fig. 12). As this element, during alteration or weathering, thorium is easily hydrolyzed and therefore has limited mobility and a tendency to concentrate in residual minerals, such as bauxite and clay minerals (Schlumberger, 1976).

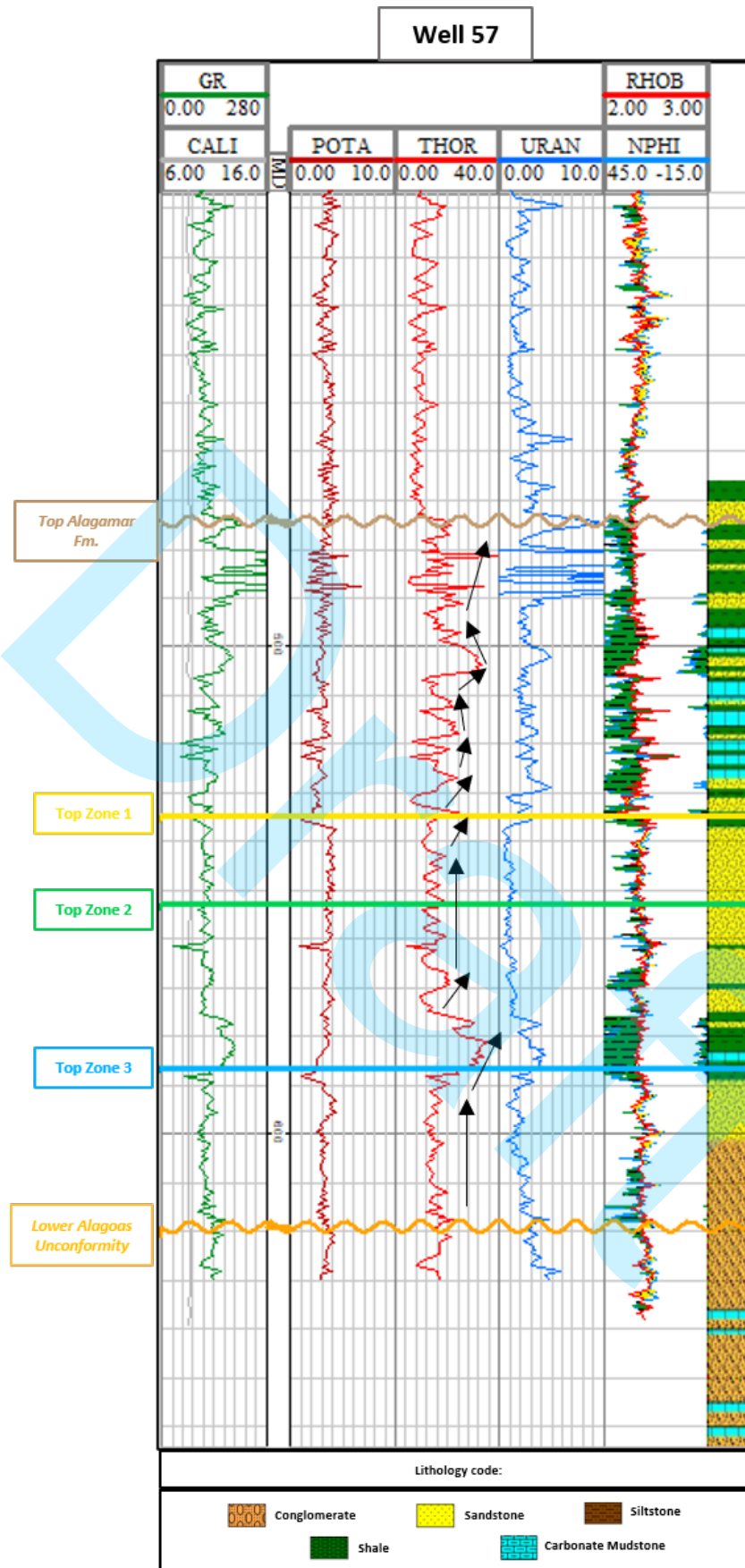


**Figure 12** – Composite log of the Well 57 showing the well tops interpreted. From track 1 to 7 the following logs are presented CALI/GR, depth, Potassium (K - %), Thorium (Th – ppm), Uranium (U –



ppm), NPHI/RHOB, and mud logging description. The top and base of Alagamar Fm., and the top of Zone 1 are well marked in the GR, NPHI, and RHOB logs. However, the reservoir zones subdivision requires radioactive concentration logs together with the conventional ones.

Using, well 57 in Figure 12, as an example, the basal zone is characterized by the high content of conglomerate, probably linked with the initial alluvial fans flows and an aggradational pattern in the Th (ppm) curve. The top is easily delimited in most of the wells by the presence of a regional shale layer with high Th (ppm) and U (ppm) values, variable thickness, and present in the mud log descriptions.

On the other hand, zones 1 and 2 are mostly composed of an intercalation of sandstones and shales with fining and coarsening upward cycles parasequences of higher stratigraphic order. As showed in Figure 8, these sandstones have high porosity and most of the hydrocarbon production comes from it. Moving away from CFS, there is higher shale content in these zones, represented by lower net sand thickness in the maps above and by the lower distance between NPHI-RHOB crossover and higher GR values in the Figure 13, and the geometry of the sand bodies is well-defined next to this fault system.

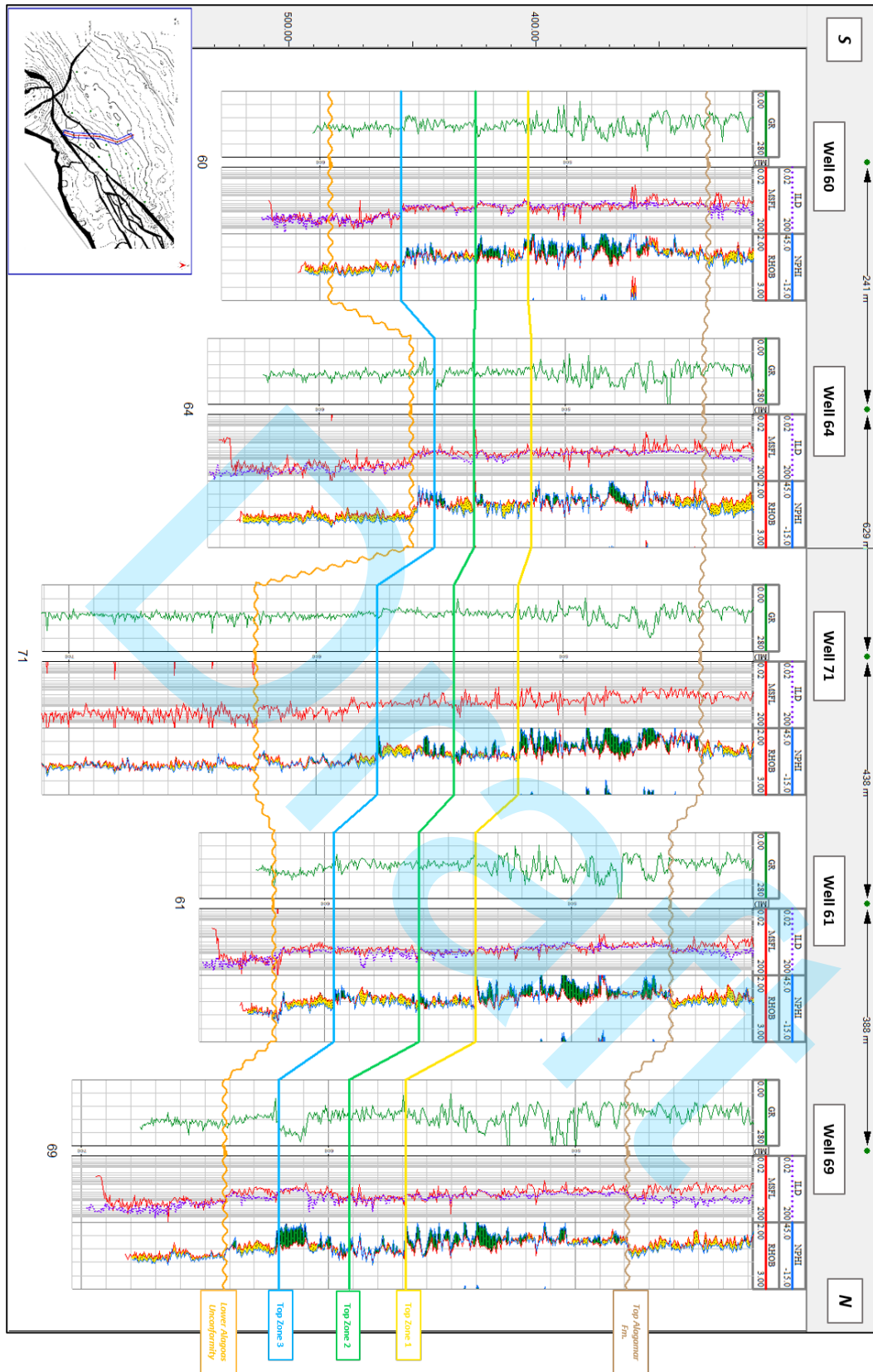


**Figure 13** – Well correlation section orientated from south to north. From Lower Alagoas Unconformity to Zone 1 Top, from Well 60 to 61, there are a few variations in the GR log, presenting a slightly serrated pattern. However, the higher shale content in the direction of Well 69, evidenced by the higher variation of this log, together with NPHI and RHOB, and by the fact that the shale, which separates Zone 3 from 2,

gets thicker, and the GR values are higher.

Above Zone 1 top, there are several thin shaly sandstones, shale beds, and carbonate mudstones, marked by the considerably higher U and Th values, that are called Ponta-Tubarão beds and well discussed by Araripe & Feijó (1994) and Pessoa Neto et al (2007).

For Zone 2 and 1, based on the Net Sand maps and  $V_{sh}$  content, the top zone had a higher water level that prevented the sand bodies from going basinward and concentrated then close to CFS. This stratigraphic tendency of higher basin water level is also evidenced by the Ponta-Tubarão beds above Zone 1.

### **Shaly intervals analysis**

For the petrophysical characterization of the clay minerals, as the wells with SGR logs are dispersed in two different portions of the studied area, there were generated three types of graphs for each reservoir zone: K (%) vs. PE (b/e) and K (%) vs. Th (ppm) (Fig. 14) based on Schlumberger (1976 & 2009), and Th/U vs. Th/K ratios (Fig. 15) based on Doveton 1994 apud Bhattacharya & Carr, 2016.

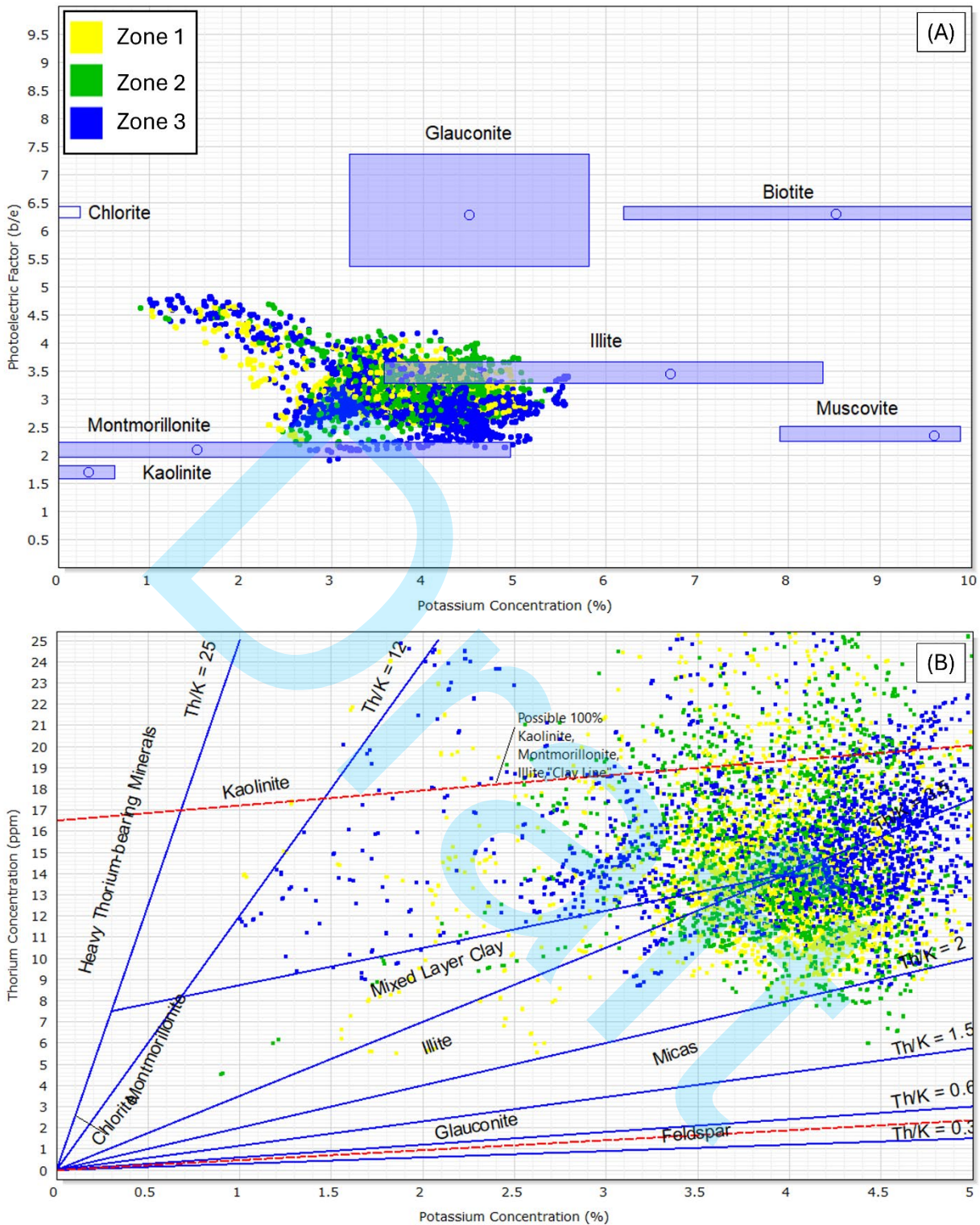


**Figure 14** – Both cross-plots have been sourced from Schlumberger (1976 and 2009) to identify the clay minerals in the reservoirs. A) Plot of K (%) vs. PE (b/e), revealing a preponderance of data points situated between ranges corresponding to illite and montmorillonite, besides that, there is a trend in the direction of chlorite that could be related to Mixed-layer clays. B) Plot of K (%) vs. Th (ppm) wherein data points also serve to indicate the presence of illite, montmorillonite, and mixed-layer clay with few points in the micas zone. This convergence of outcomes underscores the similar clay mineral composition in the study

area, alongside the equivalent impact of diagenesis therein. This figure was made using Techlog® software.

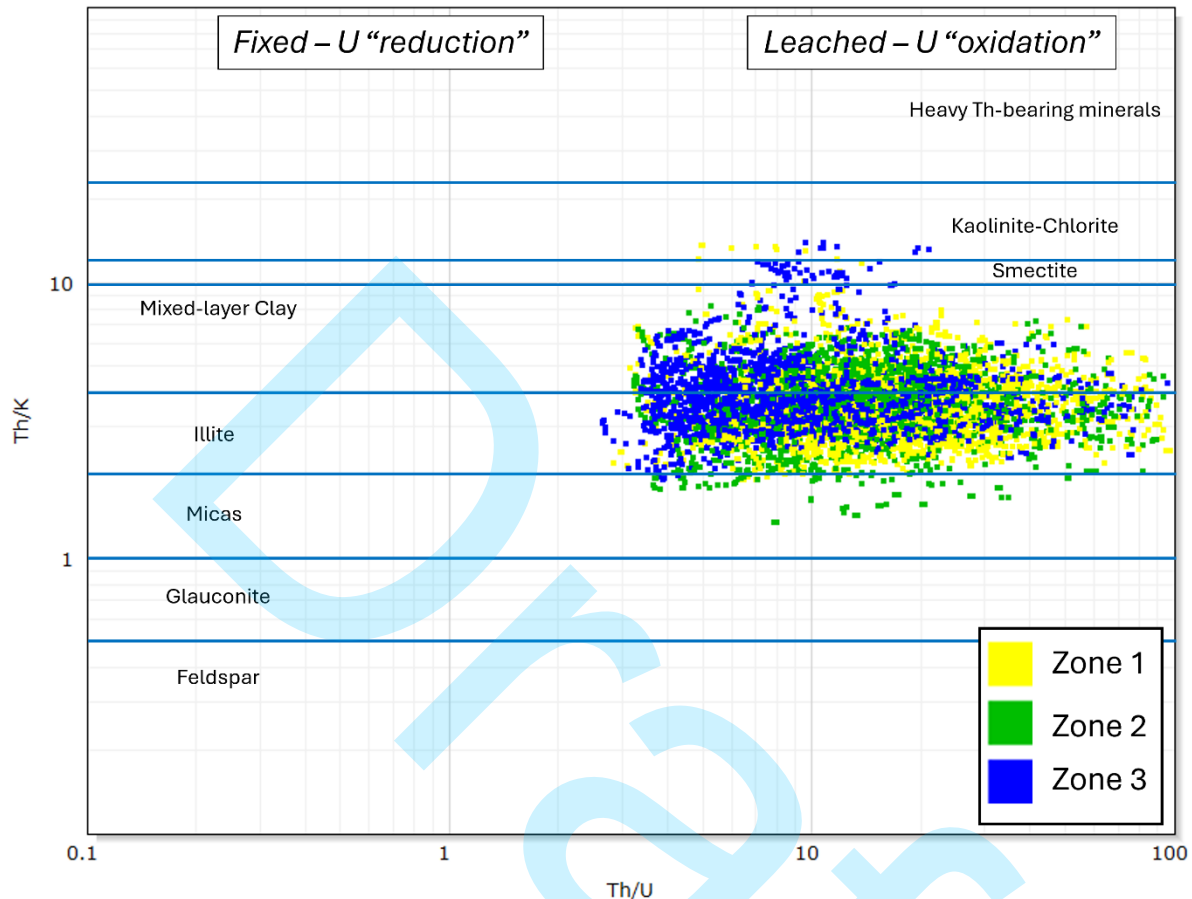


**Figure 15** – Plot Th/U vs. Th/K was initially proposed by Doveton (1994) and modified from Bhattacharya & Carr (2016). There are few differences between the reservoir zones, revealing the presence of illite, mixed-layer clay, and a small contribution of smectite, kaolinite-chlorite, and micas. These plots suggest that during the deposition phase, the prevailing depositional environment was primarily oxidizing, and it is conceivable that the uranium (U) content within the rocks underwent leaching processes. This figure was made using Techlog® software.

The first type, K (%) vs. PE (b/e), and second, K (%) vs. Th (ppm), show a high concentration of illite and few points on the montmorillonite field in both well groups. After deposition, during compaction processes, usually, montmorillonite transforms to illite, passing through an intermediary stage called mixed-layer clay (Hassan et al., 1976), and in the K (%) vs. Th (ppm) graphs, there is a tendency of some points in this intermediary clay type. So, based on these plots, we can assume that the compaction may have played an important role in this transformation.

In the context of the third type of plot, Th/U vs. Th/K, there is a concentration of data points

within the fields corresponding to illite and mixed-layer clay minerals. Additionally, a limited number of data points are situated within the domain associated with smectite clay minerals. It is noteworthy that the smectite clay does not feature in the other graphs presented.

According to Fabricius et al. (2003), in temperatures higher than 50-80°C, kaolinite and feldspars may react to form authigenic illite and quartz cement, and this process must be the source of this high concentration of illite in the reservoir zones. Furthermore, Th/U vs. Th/K plot suggests that the environment was mainly oxidizing during deposition, and the rocks' uranium (U) content underwent leaching processes.

Given the uniformity observed across all cross-plots, which consistently indicate the presence of analogous clay mineral compositions in both sectors of the study area, it is plausible to infer those diagenetic processes played a similar role within this area. When correlating the few XRD analysis data, as shown in Table 1, with the graphs, both indicated the presence of the same clay minerals, although XRD data identified a higher concentration of kaolinite than the well log plots.

After clay minerals identification, when correlating wells using SGR logs (Fig. 16), it's very clear that the K (%) log shows few variations in the three reservoir zones, and the Th (ppm) log varies a lot more. This characteristic could be associated with the shale content of the rock beds, as the amount of clay minerals gets higher, the Th (ppm) concentration also gets higher. This is evidenced by the NPHI/RHOB crossover and the mud logging that indicates shale intervals where there is high Th (ppm) content in Figure 17. Finally, calculating  $V_{sh}$  from the Th (ppm) log could be an efficient way to understand the shale content distribution in these reservoirs and identify possible stratigraphic flow barriers.

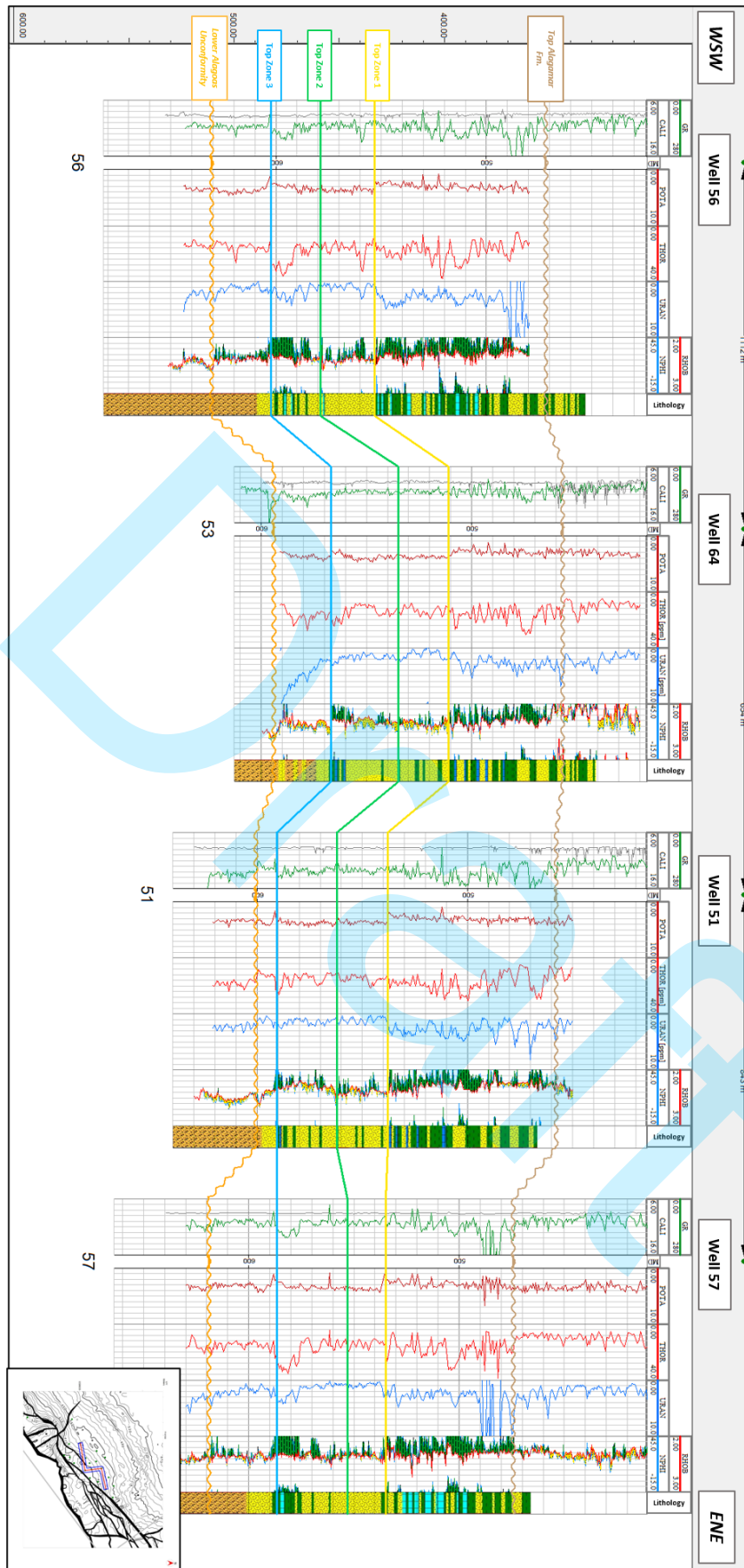


**Figure 16** – Well correlation section orientated from WSW to ENE. From Lower Alagoas Unconformity to Alagamar Formation Top, wells 56-64-51-57, there are few variations in the GR log, presenting a

slightly serrated pattern. From tracks 1 to 6, the figure shows GR, K, THOR, URAN, NPHI/RHOB, and Lithology from mud logging. The SGR logs, especially THOR, help when identifying the reservoirs' zonation, evidencing that the zones have different stacking patterns.

## CONCLUSIONS

Petrophysical reservoir characterization encompasses several different workflows using well logs and calibrating it with rock data is essential. This study proposed the integration of plug sample data with well logs to better identify the most effective method of estimation of shale volume, its impact on effective porosity calculation, when understanding the lateral continuity and geometry of the studied sand bodies, and the characterization of the clay minerals for each one of the reservoir zones contained in the Upanema Member of Alagamar Formation, yet little studied.

When it comes to identifying the most effective method to calculate shale volume in the reservoir rocks from Upanema's Member, comparing the  $\phi$  *Effective* values from plug samples and the ones calculated from well logs using the Larionov Paleogene Rocks method to estimate shale volume, showed an excellent correlation despite these rocks were deposited during Aptian-Albian. The application of this methodology for younger rocks could apply to Cretaceous rocks due to the small overburden that these rocks are submitted.

The lateral continuity and geometry of the sand bodies with good reservoir properties ( $\phi$  *Effective* > 10% and  $V_{shale}$  < 50%) were effectively identified using the Net Sand maps. It was possible to see the difference in sand dispersion between the three zones, considering that in Zone 3 the sandy sediments tend to go basinward and are more discontinuous, while in zones 1 and 2, these deposits tend to be more continuous laterally, and concentrated close to their source. This difference could be related to the water level variation at those times, resulting in the concentration of the coarse grain deposits near the Carnaubais Fault System.

Above these reservoirs, there are thicker shale deposits with higher Uranium content, which suggest a change in the deposition and environmental conditions in the Alagamar Formation, probably related to the first marine incursions described by Araripe & Feijo (1994) and Pessoa Neto et al. (2007).

Furthermore, the utilization of SGR (Spectral Gamma Ray) logs has demonstrated its efficacy not only as a method for discerning the prevalent clay mineral constituents within the reservoir zones, matching with the clays identified in the x-ray diffraction analysis qualitatively, but also giving insights about the climate conditions of the reservoir's rocks during deposition.

These logs, together with photo-electric logs, indicated a predominance of illite, mixed-layer clay, and montmorillonite compositions, with a minor presence of smectite, kaolinite-chlorite, and micas. Another interpretation is that these rocks were deposited in an oxidizing environment, probably related to low water levels.

Nonetheless, it is important to state that the most definitive approach to ascertaining the



specific clay mineral types remains through the utilization of X-ray diffraction techniques. Regrettably, such an in-depth investigation falls beyond the scope of this present paper due to the low number of samples with XRD data.

Additionally, the Thorium concentration logs with NPHI-RHOB measurements and mud logging data have proven to be an effective approach for estimating shale content. This is due to the elevated Th content observed in intervals characterized by higher shale content. So, the shale volume estimation would be better addressed using a Thorium concentration log. Unfortunately, there are few wells with this log and the correlation between rock-porosity and well-log-porosity turned out to be very effective.

## ACKNOWLEDGMENTS

This research is carried out in association with the ongoing master's degree of the corresponding author at UFF (Universidade Federal Fluminense). We thank PetroReconcavo, especially Najara Sapucaia and Gabriel Archila, for the dataset, support during this study, and technical assistance.

The authors are also grateful to the Institute of Science and Technology of Petroleum Geophysics of Brazil for supporting this research.

## REFERENCES

- Angelim, L. A. A., 2006, *Geologia e recursos minerais do estado do Rio Grande do Norte*. CPRM <https://rigeo.sgb.gov.br/handle/doc/10234>
- Anjos, S. M. C., L. F. De Ros, R. S. Souza, C. M. A. Silva, C. L. Sombra, 2000, Depositional and diagenetic controls on the reservoir quality of Lower Cretaceous Pendência sandstones, Potiguar rift basin, Brazil. *AAPG Bulletin*, v. 84, no. 11, p. 1719-1742. DOI: 10.1306/8626C375-173B-11D7-8645000102C1865D.
- Araripe, P. T., and F. J. Feijó, 1994, Bacia Potiguar. In: *Boletim de Geociências da Petrobras*, 8 (1), p. 127-141.
- Bertani, R. T., I. G., Costa, and R. M. D. Matos, 1990, *Evolução Tectono-Sedimentar, Estilo Estrutural e Hábitat do Petróleo na Bacia Potiguar*: Ed. Gávea: R. Redisch Prog. Visual Prod. Gráf. e Editoração: Petrobras, Rio de Janeiro, Brazil, p. 291-310.
- Bezerra, F. H. R. & C. Vita-Finzi, 2000, How active is a passive margin? Paleoseismicity in northeastern Brazil. *Geology* 28, 591–594.
- Bezerra, F. H., R. P. Maia, M. O. L. Sousa & G. Bertorri, 2020, Postrift stress field inversion in the Potiguar Basin, Brazil – Implications for petroleum systems and revolution of the equatorial margin of South America. *Marine and Petroleum Geology*, v. 111, p. 88-104. DOI: 10.1016/j.marpetgeo.2019.08.001.
- Bhattacharya, S. & T. Carr, 2016, Integrated Petrofacies Characterization and Interpretation of Depositional Environment of the Bakken Shale in the Williston Basin, North America. In: *Petrophysics* 57 (2).
- Bhuyan, K. & Q. Passey, 1994, Clay estimation from GR and neutron-density porosity logs. In: *Society of Petrophysicists and Well-Log Analysts (ed.), Proceedings of the SPWLA 35<sup>th</sup> Annual Logging Symposium, 19-22nd June 1994, Tulsa, Oklahoma, USA, p. 1-15.*

Clavier, C., G., Coates, and J., Dumanoir, 1984, The Theoretical and Experimental Basis for the 'Dual Water' Model for the Interpretation of Shaly Sands. Society of Petroleum Engineers Journal 24, p. 153-168. DOI: 10.2118/6859-PA.

De Castro, D. L., F. H. R. Bezerra, M. O. L. Sousa, R. A. Fuck, 2012, Influence of Neoproterozoic tectonic fabric on the origin of the Potiguar Basin, Northeastern Brazil and its links with West Africa based on gravity and magnetic data. J. Geodyn. 54, 29–42. DOI: 10.1016/j.jog.2011.09.002.

De Castro, D. L. & F. H. R. Bezerra, 2015, Fault evolution in the Potiguar rift termination, equatorial margin of Brazil. Solid Earth 6, 185–196. DOI: 10.5194/se-6-185-2015.

Doveton, J. H., 1994, Geologic Log Interpretation. In: SEPM Short Course Notes 29, p. 123-125. ISBN: 978-1565760097. DOI: 10.2110/scn.94.29.

Fabricius, I. L., L. D. Fazladic, A. Steinholm & U. Korsbech, 2003, The use of spectral natural gamma-ray analysis in reservoir evaluation of siliciclastic sediments: a case study from the Middle Jurassic of the Harald Field, Danish Central Graben. In: Geological Survey of Denmark and Greenland Bulletin 1, p. 349-366. DOI: 10.34194/geusb.v1.4677.

Hassan, M., A. Hossin & A. Combaz, 1976, Fundamentals of the Differential Gamma-ray Log: Interpretation Technique. Society of Petrophysicists and Well-Log Analysts (SPWLA).

Hill, H. J., Shirley, O. J., and Klein, G. E., 1979, Bound Water in Shaly Sands: its relation to Qv and other formation properties. The Log Analyst, 20 (3).

Juhasz, I., 1986, Assessment of the distribution of shale, porosity and hydrocarbon saturation in shaly sands, London, UK. In: 10th European Formation Evaluation Symposium, Society of Professional Well Log Analysts, Aberdeen Chapter, p. 16.

Klaja, J. & L. Dudek, 2016, Geological interpretation of spectral gamma-ray (SGR) logging in selected boreholes. In: Nafta-Gaz, 72, p. 3-14. DOI: 10.18668/NG2016.01.01.

Larionov, V. V., 1969, Borehole Radiometry Moscow, U.S.S.R. In: Nedra, M. R. L., and Biggs, W. P., Using Log-Derived Values of Water Saturation and Porosity, Trans. SPWLA Ann, Logging Symposium, 10, 26.

Matos, R. M. D., 1992, The Northeast Brazilian Rift System. Tectonics, v. 11, Issue 4, p. 766-791. DOI: 10.1029/91TC03092.

Melo, A. H., P. R. O. Andrade, A. J. C. Magalhães, D. G. C. Fragoso, F. P. Lima-Filho, 2019, Stratigraphic evolution from the early Albian to late Campanian of the Potiguar Basin, Northeast Brazil: An approach in seismic scale. In: Basin Research, 2019. DOI: 10.1111/bre.12414

Melo, A. H., A. J. C. Magalhães., M. C. Menegazzo, D. G. C. Fragoso, C. P. Florencio, and F. P. Lima-Filho, 2021, High-resolution sequence stratigraphy applied for the improvement of hydrocarbon production and reserves: A case study in Cretaceous fluvial deposits of the Potiguar basin, northeast Brazil. In: Marine and Petroleum Geology 130 (2021) 105124. DOI: 10.1016/j.marpetgeo.2021.105124

Monteiro, D. S., 2012, Sistemas deposicionais aptianos da margem sudeste da Bacia Potiguar. 2012. 69 f. Dissertação (Mestrado em Análise de Bacias;Tectônia, Petrologia e Recursos Minerais) - Universidade do Estado do Rio de Janeiro, Rio de Janeiro, 2012. Nogueira, F. C., F. H. R. Bezerra, R. A. Fuck, 2010, Quaternary fault kinematics and chronology in intraplate Northeastern Brazil. J. Geodyn. 49, 79–91. DOI: 10.1016/j.jog.2009.11.002.

Paiva, M. F. B., W. M. Lupinacci, A. F. M. Freire, and J. Hansford, 2019, Comparison of methodologies to estimate the clay content – A case study in the Roncador Field, Campos Basin.

In: 16th International Congress of the Brazilian Geophysical Society, Rio de Janeiro, Brazil, 19-22 August 2019. DOI: 10.22564/16cisbgf2019.091.

Pessoa Neto, O. C., U.M., Soares, J. G. F., Silva, E.H., Roesner, C. P., Florencio, C. A. V. Souza, 2007. Bacia Potiguar. In: Boletim de Geociências da Petrobras 15 (2), p. 357-369.

Schlumberger, 1974, Log Interpretation Manual/Applications. Vol. 2. Schlumberger Well Service, Inc., Houston.

Schlumberger, 1976, Natural Gamma Ray Spectrometry: Essentials of N.G.S. Interpretation. Schlumberger Education Services, Houston.

Schlumberger, 1987, Log Interpretation Principles/Applications. Schlumberger Education Services, Houston.

Schlumberger, 2009, Log Interpretation Charts. Schlumberger Education Services, Houston.

Serra, O., J. Baldwin, J. Quirein, 1980, Theory, Interpretation, and Practical Applications of Natural Gamma-ray Spectroscopy. In: SPWLA 21<sup>st</sup> Annual Logging Symposium, Lafayette, Louisiana, USA.

Stieber, S. J., 1970, Pulsed Neutron Capture Log Evaluation – Louisiana Gulf Coast. In: Fall Meeting of the Society of Petroleum Engineers of AIME, Houston, Texas, 4-7 October 1970. DOI: 10.2118/2961-MS

This article is part of **Ferreira, V.** Master's degree research, with **Freire, A.** as the primary advisor and **Lupinacci, W.** as the co-supervisor. **Ferreira, V.** generated all the results, and the discussions and conclusions were developed collaboratively with all co-authors.